# Stability and Electronic Properties of $TiO_2$ Nanostructures With and Without B and N Doping

D. J. Mowbray,* J. I. Martinez, J. M. García-Lastra, K. S. Thygesen, and K. W. Jacobsen
*Center for Atomic-scale Materials Design, Department of Physics,*
*Technical University of Denmark, DK-2800 Kgs. Lyngby, Denmark*
(Received January 8, 2009; Published June 19, 2009)

We address one of the main challenges to $TiO_2$-photocatalysis, namely band gap narrowing, by combining nanostructural changes with doping. With this aim we compare $TiO_2$'s electronic properties for small 0D clusters, 1D nanorods and nanotubes, 2D layers, and 3D surface and bulk phases using different approximations within density functional theory and GW calculations. In particular, we propose very small ($R \lesssim 5$ Å) but surprisingly stable nanotubes with promising properties. The nanotubes are initially formed from $TiO_2$ layers with the $PtO_2$ structure, with the smallest (2,2) nanotube relaxing to a rutile nanorod structure. We find that quantum confinement effects – as expected – generally lead to a widening of the energy gap. However, substitutional doping with boron or nitrogen is found to give rise to (meta-)stable structures and the introduction of dopant and mid-gap states which effectively reduce the band gap. Boron is seen to always give rise to $n$-type doping while depending on the local bonding geometry, nitrogen may give rise to $n$-type or $p$-type doping. For undercoordinated $TiO_2$ surface structures found in clusters, nanorods, nanotubes, layers and surfaces nitrogen gives rise to acceptor states while for larger clusters and bulk structures donor states are introduced.

arXiv:1001.2573v1 [cond-mat.mtrl-sci] 14 Jan 2010

## I. INTRODUCTION

Motivated by the world's ever increasing need for cleaner burning fuels and more viable forms of renewable energy, hydrogen production via photocatalysis has been intensely researched as a possible candidate for addressing these issues. Since the first experimental formation of hydrogen by photocatalysis in the early 1980s [1], $TiO_2$ has been the catalyst of choice. Reasons for this include the position of $TiO_2$'s conduction band above the energy of hydrogen formation, the relatively long lifetime of excited electrons which allows them to reach the surface from the bulk, $TiO_2$'s high corrosion resistance compared to other metal oxides, and its relatively low cost [2–4].

However, the large band gap of bulk $TiO_2$ ($\approx 3$ eV) means that only high energy UV light may excite its electrons. This effectively blocks most of the photons which pierce the atmosphere, typically in the visible range, from participating in any bulk $TiO_2$ based photocatalytic reaction. On the other hand, the difference in energy between excited electrons and holes, i.e. the band gap, must be large enough ($\gtrsim 1.23$ eV) to dissociate water into hydrogen and oxygen. For these reasons it is of great interest to adjust the band gap $\varepsilon_{gap}$ of $TiO_2$ into the range $1.23 \lesssim \varepsilon_{gap} \lesssim 2.5$ eV, while maintaining the useful properties mentioned above [5].

With this aim, much research has been done on the influence of $TiO_2$ nanostructure [6–10] and dopants [5, 11–17] on photocatalytic activity. For low dimensional nanostructured materials, electrons and holes have to travel shorter distances to reach the surface, allowing for a shorter quasi-particle lifetime. However, due to quantum confinement effects, lower dimensional $TiO_2$ nanostructures tend to have *larger* band gaps [18]. On the other hand, although doping may introduce mid-gap states, recent experimental studies have shown that boron and nitrogen doping of bulk $TiO_2$ yields band gaps *smaller* than the threshold for water splitting [11, 12]. This suggests that low dimensional structures with band gaps larger than about 3.0 eV may be a better starting point for doping.

The experimental synthesis and characterization of nanostructured materials is in general a costly and difficult task. On the other hand, modern electronic structure modelling has reached a level where large-scale calculations can provide realistic descriptions of structure and electronic properties.

Based on our investigation, we suggest as a promising candidate small ($R \lesssim 5$ Å) $TiO_2$ nanotubes, with a hexagonal ABC $PtO_2$ structure (HexABC), which we find to be surprisingly stable, even in the boron and nitrogen doped forms. This stability may be attributed to their structural similarity to bulk rutile $TiO_2$, with the smallest nanotube having the same structure as a rutile nanorod.

A further difficulty for any photocatalytic system is controlling how electrons and holes travel through the system [19]. For this reason, methods for reliably producing both $n$-type and $p$-type $TiO_2$ semiconducting materials are highly desirable. So far, doped $TiO_2$ tends to yield only $n$-type semiconductors. We propose that $p$-type $TiO_2$ semiconducting materials may be obtained by nitrogen doping surface sites of low dimensional materials.

In this study we report the results of density functional theory (DFT) and GW calculations of the energetic stability and electronic structure of recently suggested $(TiO_2)_n$ clusters ($n \leq 9$) [6] and novel ($n$,$n$) $TiO_2$ nanotubes ($n \leq 4$) in the undoped, boron doped, and nitrogen doped forms. The formation energy $E_{form}$, density of states (DOS), and energy gap $\varepsilon_{gap}$, for these systems are compared with that for 2D HexABC and anatase layers, and 3D $TiO_2$ anatase surface, anatase bulk, and rutile bulk phases. Furthermore, we analyze how boron and nitrogen doping influences the DOS for these systems, and how their nanostructure may determine whether the resulting semiconductor is $n$-type or $p$-type.

In Sec. II we describe the DFT and GW methodologies used to obtain the energies and electronic structure of the studied systems. We compare the energetic stability of the systems in Sec. III. In Sec. IV we discuss the electronic structures of

*Electronic address: dmowbray@fysik.dtu.dk

the systems, showing the DOS and energy gaps, followed by a concluding section.

## II. METHODOLOGY

All DFT calculations have employed the RPBE exchange correlation (xc)-functional [20]. The plane-wave code DACAPO[21, 22] was used for structural minimization, the real-space code OCTOPUS[23] for charged calculations, and YAMBO[24] with ABINIT[25] or PWSCF[26] for GW calculations. A plane-wave cutoff of 340 eV was used, with a Monkhorst-Pack **k**-point sampling of $1\times1\times12$ for $TiO_2$ nanotubes, where the nanotube axis is parallel to the $z$-axis, $12\times12\times1$ for $TiO_2$ layers and surfaces, where the normal direction is parallel to the $z$-axis, and $12\times12\times12$ for $TiO_2$ bulk phases. All structures have been relaxed until a maximum force below 0.04 eV/Å was obtained. The occupation of the one electron states was calculated at a temperature of $k_BT$ ≈0.1 eV for the periodic systems and $k_BT$ ≈0.01 eV for the clusters, with all energies extrapolated to $T$ =0 K. Spin unpolarized calculations have been performed for the undoped $TiO_2$ systems, while spin polarized calculations have been performed for all doped $TiO_2$ systems, since the unit cells for the doped systems contain an odd number of electrons.

Doping of $(TiO_2)_n$ clusters has been modeled by substituting a single boron or nitrogen atom in each geometrically inequivalent oxygen site of the most stable isomer to determine the most stable doping site. Only clusters of sufficient size to obtain experimentally realizable doping fractions $\lesssim 10\%$ ($5 \le n \le 9$) have been considered [11–15].

To model $TiO_2$ nanotube doping, we have repeated the minimal unit cell four times along the tube axis, and substituted a single boron or nitrogen atom in each geometrically inequivalent oxygen site to obtain the most stable doped structure. In this way, dopant-dopant interactions are minimized by maintaining a dopant separation of approximately 12 Å. This corresponds to experimentally realizable doping fractions of 3.1%, 2.1%, and 1.6% for $TiO_2$ (2,2) nanorods, (3,3) nanotubes and (4,4) nanotubes, respectively.

Doping of $TiO_2$ layers, surfaces, and bulks has been similarly modeled by repeating the minimal unit cell twice in each periodic direction, and substituting a single boron or nitrogen atom in each geometrically inequivalent oxygen site to obtain the most stable structure. Experimentally realizable doping fractions of 5.6%, 3.1%, and 3.1% were thus obtained for the layers, surfaces, and bulks respectively.

## III. ENERGETIC STABILITY

We define the formation energy $E_{form}$ for a given structure consisting of $n$ $TiO_2$ functional units as

$$E_{form} = \frac{1}{n}E[\mathrm{Ti}_n\mathrm{O}_{2n-p-q}\mathrm{B}_p\mathrm{N}_q] - E[\mathrm{TiO_2}] - \frac{1}{n}\left(pE[\mathrm{B}] + qE[\mathrm{N}] - (p+q)E[\mathrm{O}]\right), \quad (1)$$

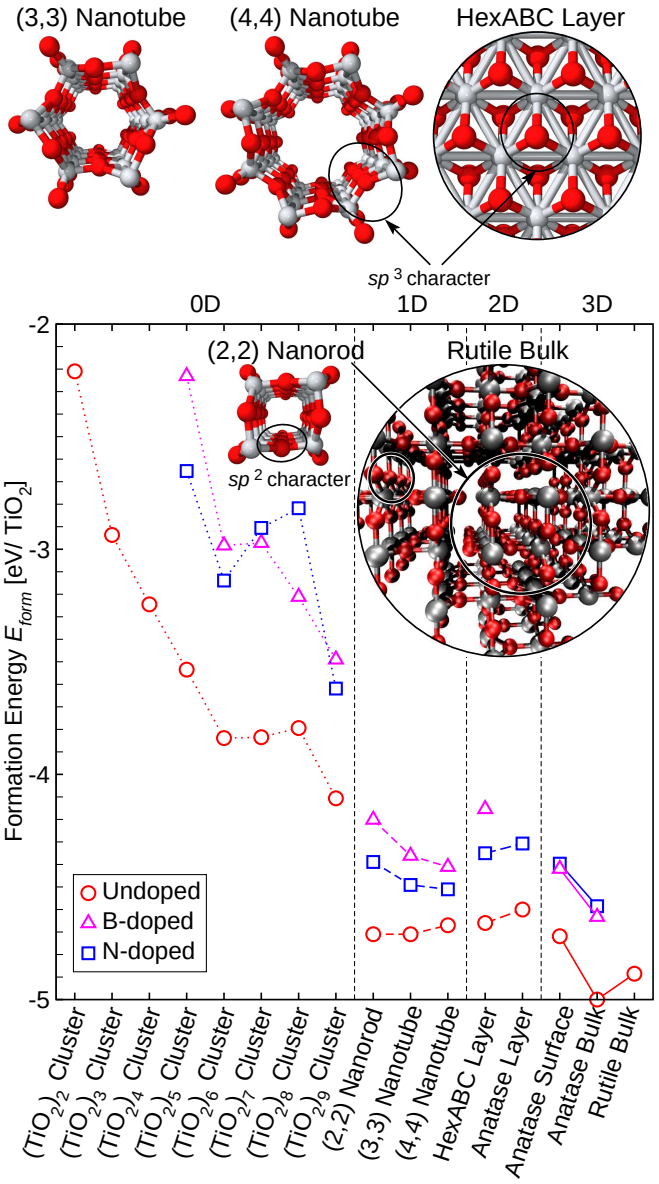



FIG. 1: Formation energy $E_{form}$ in eV per $TiO_2$ functional unit versus $TiO_2$ structure for 0D $(TiO_2)_n$ clusters ($n \le 9$), 1D $TiO_2$ (2,2) nanorods, (3,3) nanotubes, and (4,4) nanotubes, 2D HexABC and anatase layers, and 3D anatase surface, anatase bulk, and rutile bulk phases. DFT calculations using RPBE for the undoped (○, red), nitrogen doped (□, blue), and boron doped (△, magenta) systems are shown. Note the $sp^2$ character of oxygen in the more stable rutile and (2,2) nanorod structure, and the $sp^3$ character of oxygen in the less stable layer and larger nanotube structures.

where $E[\mathrm{Ti}_n\mathrm{O}_{2n-p-q}\mathrm{B}_p\mathrm{N}_q]$ is the total energy for the system, $E[\mathrm{TiO_2}]$ is the energy of an isolated $TiO_2$ molecule, and $E[\mathrm{O}]$, $E[\mathrm{B}]$, and $E[\mathrm{N}]$ are the respective energies with reference to gas phase species for O, B, and N. These have been obtained using the experimental doping reactions

$$E[\mathrm{O}] = E[\mathrm{H_2O}] - E[\mathrm{H_2}] - \Delta H[\mathrm{H_2O}], \quad (2)$$

$$E[\mathrm{B}] = \frac{1}{2}\left(E[\mathrm{B_2H_6}] - 3E[\mathrm{H_2}] - \Delta H[\mathrm{B_2H_3}]\right), \quad (3)$$

$$E[\mathrm{N}] \;=\; \frac{1}{2}E[\mathrm{N_2}], \tag{4}$$

where the formation reaction enthalpies are $\Delta H[\mathrm{H_2O}] \approx -2.506$ eV and $\Delta H[\mathrm{B_2H_6}] \approx 0.377$ eV, as taken from Ref. [27]. This avoids difficulties associated with modeling isolated atoms and the triplet state of molecular oxygen.

Fig. 1 shows DFT calculated formation energies $E_{form}$ for undoped, boron doped, and nitrogen doped forms of 0D $(\mathrm{TiO_2})_n$ clusters ($n \leq 9$), 1D $(n,n)$ nanotubes ($n \leq 4$), 2D HexABC and anatase layers, and 3D anatase surface, anatase bulk, and rutile bulk phases.

From the formation energies, we see that $(\mathrm{TiO_2})_n$ clusters become generally more stable with increasing size, as expected. On the other hand, the formation energies of the $(n,n)$ $\mathrm{TiO_2}$ nanotubes ($n \leq 4$) suggest that they are all surprisingly stable, being more stable than the 2D structures and within approximately 0.2 eV of the least stable bulk phases. Even more surprising, the $\mathrm{TiO_2}$ nanotubes seem to become more stable with *decreasing* size. This is clearly seen in Fig. 2, which shows the radial dependence of the formation energies for the $\mathrm{TiO_2}$ (2,2) nanorod and $\mathrm{TiO_2}$ $(n,n)$ nanotubes ($3 \leq n \leq 8$).

In a simple classical picture, the strain energy to be overcome when bending a layer into a tube should be inversely proportional to the square of the tube radius ($\sim R^{-2}$). Such models have been shown to accurately describe $\mathrm{TiO_2}$ anatase and lepidocrocite layer nanotubes [28]. However, the HexABC $\mathrm{TiO_2}$ nanotube system is complicated by the fact that $\mathrm{TiO_2}$ is not found naturally in a HexABC layered structure. As a result, the strain energy introduced by bending the layer may be overcome by changes in bonding which better resemble the bulk $\mathrm{TiO_2}$ structures. This is seen in Fig. 1, where we find oxygen atoms have $sp^3$ character in both the infinite layer structure and the (4,4) $\mathrm{TiO_2}$ nanotube, but $sp^2$ character in the more stable bulk rutile and (2,2) $\mathrm{TiO_2}$ nanorod.

As shown in Fig. 2, the radial dependence of the nanotube formation energies may be well approximated by

$$E_{form} \;=\; E_{layer} + (E_{rutile} - E_{layer})R_{(2,2)}/R. \tag{5}$$

Here $E_{layer} \approx 4.63$ eV/$\mathrm{TiO_2}$ is the formation energy of the nanotube layer calculated using the optimized unit cell parameters for the nanotubes, $E_{rutile} \approx 4.89$ eV/$\mathrm{TiO_2}$ is the formation energy of the bulk rutile phase, $R_{(2,2)}$ is the radius of a $\mathrm{TiO_2}$ (2,2) nanorod, and $R$ is the nanotube radius. The first term in (5) ensures the nanotube formation energy tends to that for the infinite layer at large nanotube radii. The second term models the increase in stability as the nanotube is 'bent' into a more rutile-like structure at smaller radii. This reaches a maximum for a (2,2) nanorod ($R = R_{(2,2)}$), where the structure becomes that of the rutile phase.

It should be noted that DFT formation energies have been shown to not accurately describe the relative stability of anatase and rutile phases, independent of xc-functional used [29]. This should be borne in mind when comparing formation energies.

Comparison of the doped formation energies with those of the undoped $\mathrm{TiO_2}$ structures shows that although less stable, doped forms of both $\mathrm{TiO_2}$ clusters and nanotubes should be experimentally realizable. This is further justified by recent nitrogen doping experiments of large $\mathrm{TiO_2}$ nanotubes which yielded doping fractions between 1% and 10% [12, 14, 15].

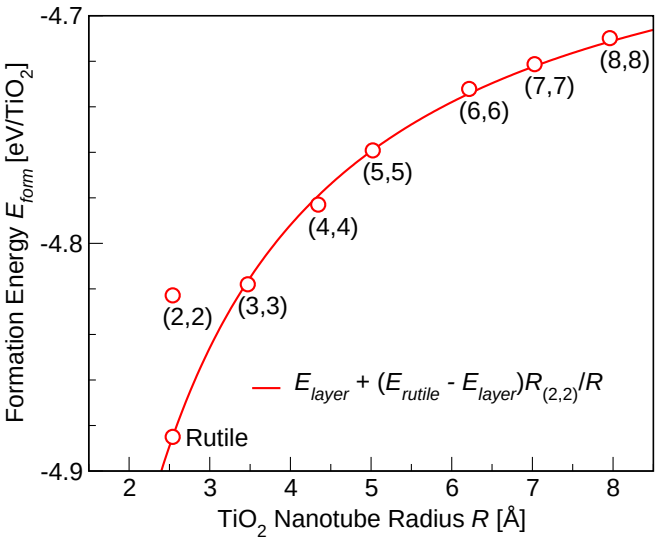



FIG. 2: Formation energy $E_{form}$ in eV per $\mathrm{TiO_2}$ functional unit versus radius $R$ in Å for $\mathrm{TiO_2}$ (2,2) nanorods and $(n,n)$ nanotubes ($3 \leq n \leq 8$) (○, red). For comparison, the $\mathrm{TiO_2}$ nanotube formation energies are also approximated by $E_{form} \approx E_{layer} + (E_{rutile} - E_{layer})R_{(2,2)}/R$, (———, red), where $R_{(2,2)}$ ≈2.54 Å is the radius of a $\mathrm{TiO_2}$ (2,2) nanorod.

The formation energies of the doped systems also appear to correlate well with both those of the undoped structures, and the relative doping fraction. Further, structures are typically less stable when doping induces oxygen dislocations, which occur for boron and nitrogen doped $(\mathrm{TiO_2})_7$ clusters, $(\mathrm{TiO_2})_8$ clusters, and bulk phases. On the other hand, systems are more stable when the $\mathrm{TiO_2}$ structure is unchanged by the introduction of a dopant, as is the case for nitrogen doping of $(\mathrm{TiO_2})_n$ clusters with surface sites ($n = 5, 6, 9$), nanotubes, layers, and surfaces. Such a distinction will also prove useful when we analyze the electronic structure of the doped systems in Sec. IV.

## IV. ELECTRONIC STRUCTURE

### A. DOS of 0D Clusters

We shall begin our analysis of the electronic structure of boron and nitrogen doped $\mathrm{TiO_2}$ nanostructures by first considering $(\mathrm{TiO_2})_n$ clusters ($5 \leq n \leq 9$). As well as being of interest in its own right, the study of such systems provides insight into how local changes in nanostructure may change whether a dopant behaves as a donor or acceptor site. Such information will prove useful when trying to form $p$-type $\mathrm{TiO_2}$ semiconducting materials.

The DFT calculated DOS and structures for the most stable boron and nitrogen doped $(\mathrm{TiO_2})_n$ clusters are shown in Figs. 3 and 4, for $5 \leq n \leq 9$. In general, boron prefers to replace the most highly coordinated oxygen in $\mathrm{TiO_2}$ clusters,

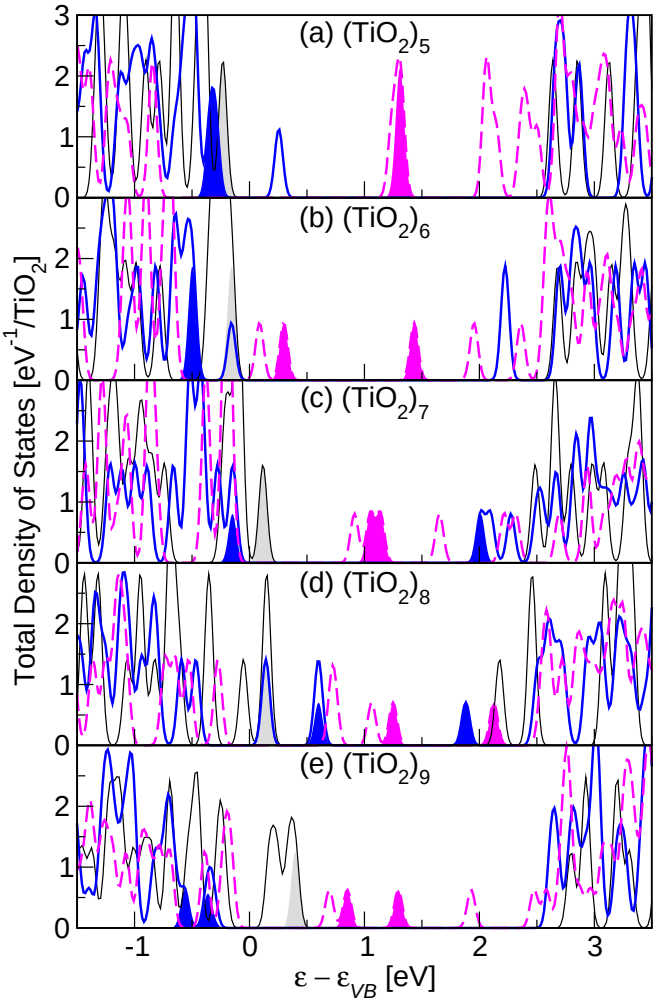



FIG. 3: Total density of states in $eV^{-1}$ per $TiO_2$ functional unit versus energy in eV for undoped (thin black solid line), boron doped (magenta dashed line) and nitrogen doped (blue thick solid line) (a–e) $(TiO_2)_n$ clusters for $5 \leq n \leq 9$, with doping fractions of $1/2n$. Energies are measured from the top of the valence bands of anatase $TiO_2$ $\varepsilon_{VB}$, and the DOSs are shifted to align the lowest eigenstate with that for anatase $TiO_2$. Occupancy is denoted by curve filling for states in the band gap.

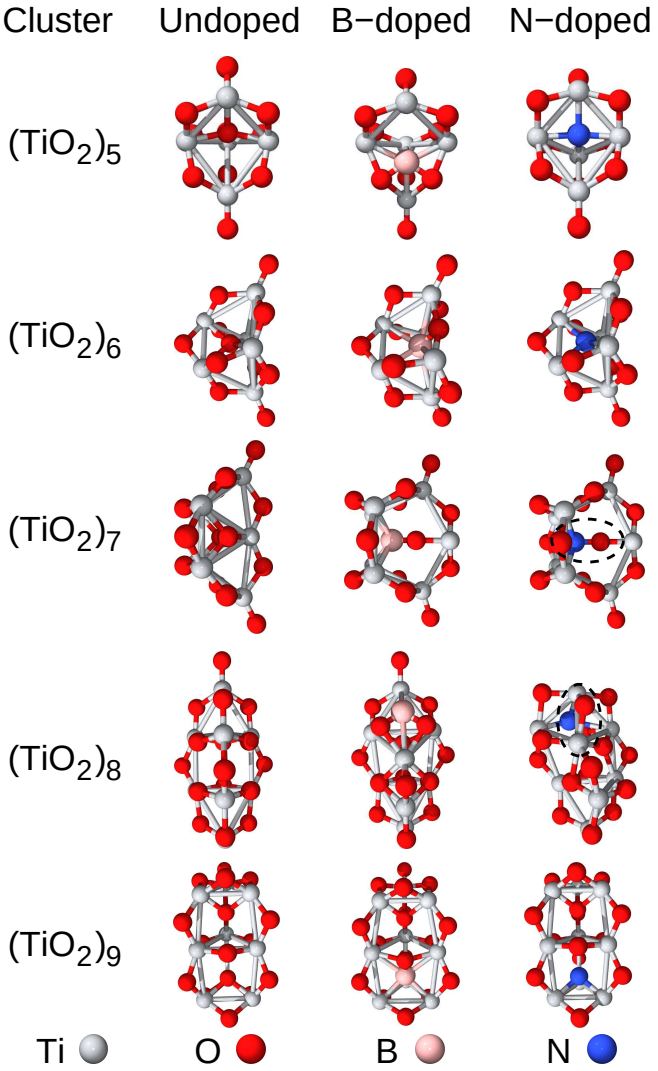



FIG. 4: Schematics of undoped (left), boron doped (middle), and nitrogen doped (right) $(TiO_2)_n$ clusters for $5 \leq n \leq 9$, with doping fractions of $1/2n$. Note the circled nitrogen-oxygen bonds in the nitrogen doped structures for $n = 7$ and 8, where nitrogen acts as a donor [6].

typically in a central location, and forms boron-oxygen bonds via oxygen dislocations, as shown in Fig. 4. Due to its electropositive character, boron acts as a donor, introducing three occupied mid-gap states near the lowest unoccupied molecular orbital (LUMO), as seen in Fig. 3.

However, for $(TiO_2)_n$ clusters the influence of nitrogen dopants is not as straightforward. As with rutile $TiO_2$ surfaces[16, 17], nitrogen prefers to occupy sites which are 3-fold coordinated to titanium. For clusters consisting only of surface sites ($n = 5$, 6, 9), oxygen is tightly constrained, and no significant changes in the cluster's structure occur via oxygen dislocations, as shown in Fig. 4. As with rutile $TiO_2$ surfaces[16, 17], nitrogen acts as an acceptor, introducing an unoccupied mid-gap state near the highest occupied molecular orbital (HOMO).

For clusters where the nitrogen dopant's oxygen neighbors occupy interior/bulk sites ($n = 7$, 8), oxygen is more mobile, and may form new nitrogen-oxygen bonds, as shown in Fig. 4. Since oxygen is more electronegative than nitrogen, nitrogen may transfer charge to the bonding oxygen through these bonds. In this case, nitrogen instead acts as a donor, introducing occupied states near the LUMO.

In general, we find when dopants form bonds with oxygen atoms via oxygen dislocations, they act as donor sites. On the other hand, when dopants such as nitrogen leave the $TiO_2$ structure unchanged, they act as acceptor sites, yielding a somewhat more stable structure. We shall find such a description useful in understanding why nitrogen dopants behave differently in low dimensional systems and bulk systems.

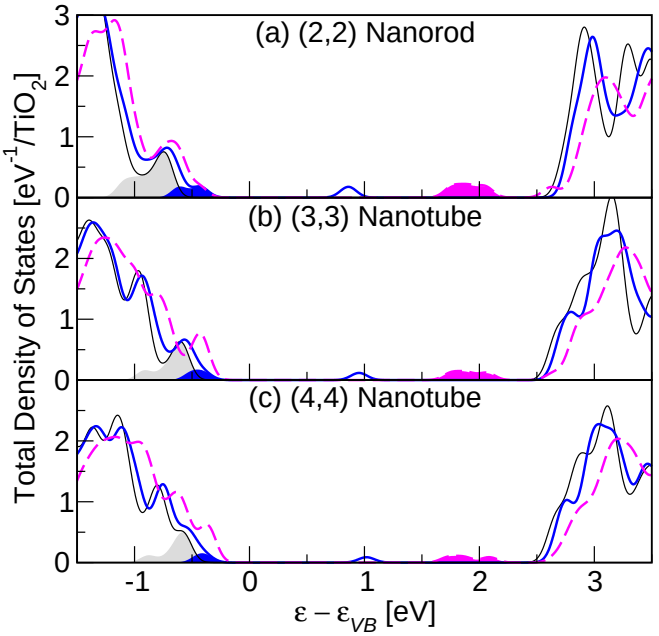



FIG. 5: RPBE calculation of the total density of states in eV$^{-1}$ per $TiO_2$ functional unit versus energy in eV for undoped (thin black solid line), boron doped (magenta dashed line) and nitrogen doped (blue thick solid line) $TiO_2$ (a) (2,2) nanorods, (b) (3,3) nanotubes and (c) (4,4) nanotubes, with 3.1%, 2.1%, and 1.6% doping respectively. Energies are measured from the top of the valence bands of anatase $TiO_2$ $\varepsilon_{VB}$, and the DOSs are shifted to align the lowest eigenstate with that for anatase $TiO_2$. Occupancy is denoted by curve filling for states in the band gap.

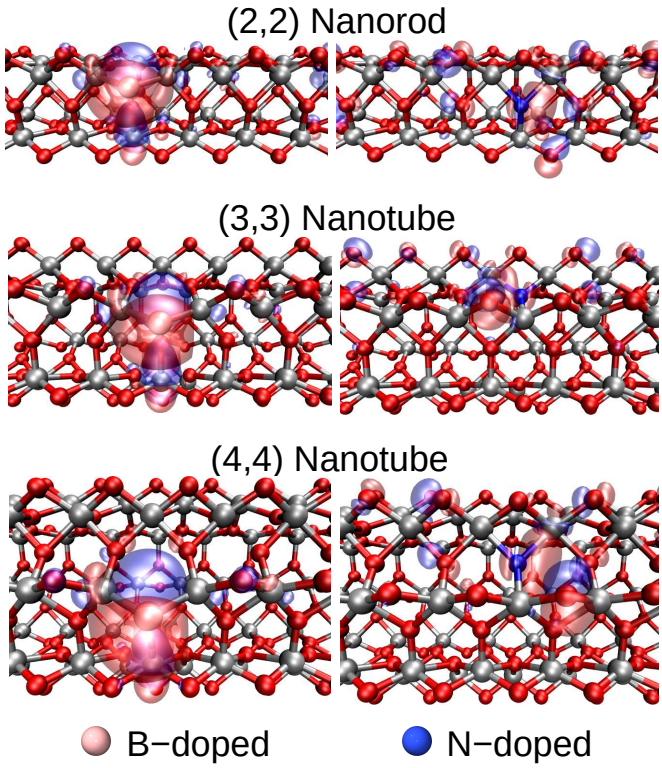



FIG. 6: Schematics of boron doped (left) and nitrogen doped (right) $TiO_2$ (2,2) nanorods, (3,3) nanotubes, and (4,4) nanotubes, with 3.1%, 2.1%, and 1.6% doping respectively. The highest occupied states for boron and nitrogen doped $TiO_2$ 1D structures are depicted by isosurfaces of $\pm 0.05 e/\text{Å}^3$.

### B. DOS of 1D Nanorods and Nanotubes

We shall now discuss how boron and nitrogen doping influences the electronic structure of stable 1D nanorods and nanotubes. Although the the most stable doping sites are the same as those obtained for doped $TiO_2$ rutile surface and bulk [5, 16, 17], the influence of dopants on the DOS is rather different.

Figure 5 shows the DFT calculated DOS and Fig. 6 the structures of the most stable boron doped and nitrogen doped $TiO_2$ (2,2) nanorods, (3,3) nanotubes, and (4,4) nanotubes. The highest occupied state is also shown as isosurfaces of $\pm 0.05 e/\text{Å}^3$ in the side views of the doped structures.

As with $TiO_2$ clusters, the influence of boron dopants on $TiO_2$ nanorods and nanotubes may be understood in terms of boron's weak electronegativity, especially when compared with the strongly electronegative oxygen. We find that boron prefers to occupy oxygen sites which are 2-fold coordinated to neighboring titanium atoms. However, as with the 0D clusters, boron's relatively electropositive character induces significant structural changes in the 1D structures, creating a stronger third bond to a neighboring three-fold coordinated oxygen via an oxygen dislocation, as shown in Fig. 5. This yields three occupied mid-gap states localized on the boron dopant, which overlap both the valence band O $2p_\pi$ and conduction band Ti $2d_{xy}$ states, as shown in Fig. 5. Boron dopants

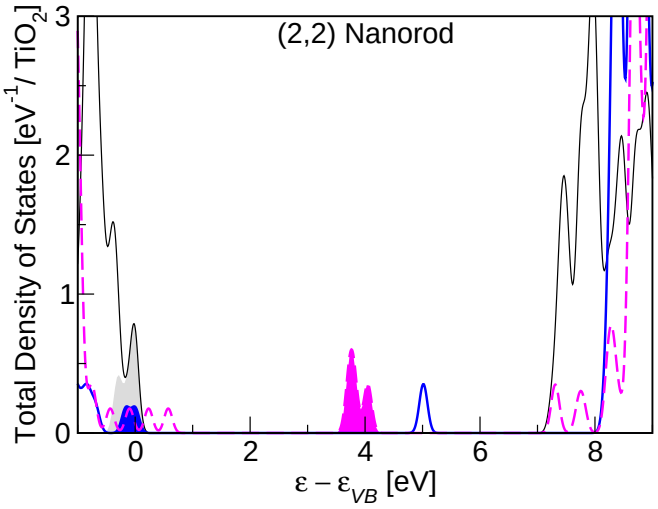
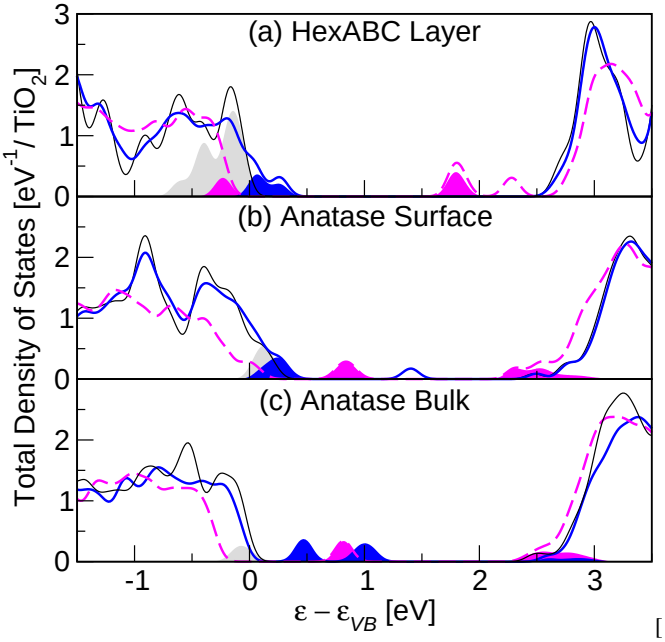



FIG. 7: GW calculation of the total density of states in eV$^{-1}$ per $TiO_2$ functional unit versus energy in eV for undoped (thin black solid line), boron doped (magenta dashed line) and nitrogen doped (blue thick solid line) $TiO_2$ (2,2) nanorods with 3.1% doping. Energies are measured from the top of the valence bands of the undoped $TiO_2$ nanorod $\varepsilon_{VB}$, and the DOSs are shifted to align the lowest eigenstate with that for the undoped $TiO_2$ nanorod. Occupancy is denoted by curve filling for states in the band gap.




[!b]

FIG. 8: Total density of states in eV$^{-1}$ per $TiO_2$ functional unit versus energy in eV for undoped (thin black solid line), boron doped (magenta dashed line) and nitrogen doped (blue thick solid line) (a) $TiO_2$ HexABC layer, (b) $TiO_2$ anatase surface, and (c) bulk anatase, with 5.6%, 3.1%, and 3.1% doping respectively. Energies are measured from the top of the valence bands of anatase $TiO_2$ $\varepsilon_{VB}$, and the DOSs are shifted to align the lowest eigenstate with that for anatase $TiO_2$. Occupancy is denoted by curve filling for states in the band gap.

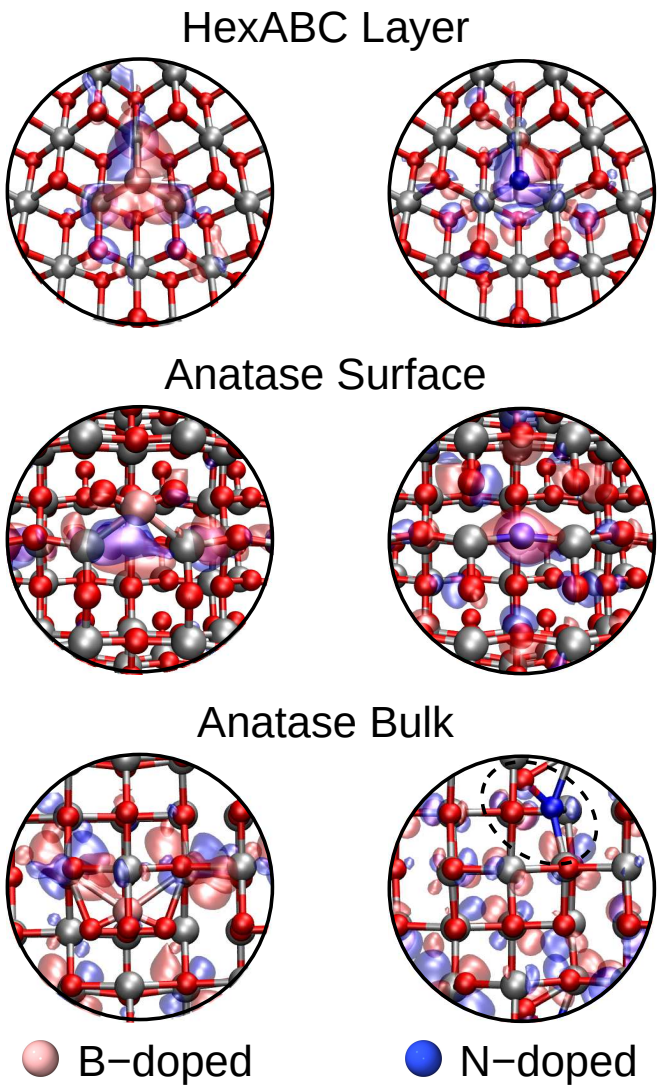



FIG. 9: Schematics of the boron doped (left) and nitrogen doped (right) HexABC layer, anatase surface, and anatase bulk phases, with 5.6%, 3.1%, and 3.1% doping respectively. The highest occupied states for boron and nitrogen doped $TiO_2$ 2D and 3D structures are depicted by isosurfaces of $\pm 0.05 e/\text{Å}^3$. Note the circled nitrogen-oxygen bonds in the nitrogen doped structures for the bulk phase, where nitrogen acts as a donor [6].

thus yield donor states near the conduction band, which may be photocatalytically active in the visible region. However, the quantum confinement inherent in these 1D structures may stretch these gaps, as found for the GW calculated DOS shown in Fig. 7.

On the other hand, we find nitrogen dopants prefer to occupy oxygen sites which are 3-fold coordinated to Ti, as was previously found for the rutile $TiO_2$ surface[16, 17]. This yields one occupied state at the top of the valence band and one unoccupied mid-gap state in the same spin channel. Both states are localized on the nitrogen dopant but overlap the valence band O $2p_\pi$ states, as shown in Fig. 6. Nitrogen dopants thus act as acceptors, providing localized states well above the valence band, as is also found for the GW calculated DOS shown in Fig. 7.

Although we find nitrogen dopants act as acceptors in $TiO_2$ 1D structures, such large gaps between the valence band and the unoccupied mid-gap states would not yield $p$-type semiconductors. This may be attributed to the substantial quantum confinement in these 1D structures. However, for 2D and 3D systems, we find it is possible to produce both $p$-type and $n$-type classical semiconductors.

### C. DOS of 2D Layers, 3D Surfaces and Bulks

To determine the reliability of our DFT and GW electronic structure calculations, we now consider the influence of boron and nitrogen doping on the DOS for 2D and 3D $TiO_2$ structures, which may be compared with recent experiments.

For the HexABC layer shown in Figs. 8(a) and 9, boron and nitrogen dopants act as donors and acceptors respectively, as was the case for the $TiO_2$ nanotubes. However, for these 2D structures the doping states are sufficiently close in energy to the conduction band or valence band to allow charge transfer for classical $n$-type or $p$-type doping by boron or nitrogen dopants respectively. A similar behavior is found for

the anatase surface, shown in Fig. 8(b) and Fig. 9. This suggests boron and nitrogen doped 2D $TiO_2$ layers or surfaces may potentially be used for $TiO_2$ based electronics.

On the other hand, for bulk anatase boron and nitrogen dopants both yield $n$-type semiconductors, as is seen experimentally [13]. We attribute this difference to the nitrogen-oxygen bond shown in Fig. 8(c), which may arise due to oxygen's greater structural flexibility in the bulk. As a result, boron and nitrogen doping both yield mid-gap occupied Ti $2d_{xy}$ conduction band states with little weight on the doping sites. Here, the dopants donate their valence electrons fully to the conduction band, as seen in Fig. 8(c).

Nitrogen thus acts as a donor for bulk-like clusters and anatase, in agreement with recent findings for nitrogen doping of both bulk anatase and thick bulk-like anatase nanopores [13]. This suggests that $n$-type or $p$-type semiconductors may be produced by nitrogen doping depending on whether nearby oxygen atoms occupy lower-coordinated surface or higher-coordinated bulk sites.

Further, we also find that the highest occupied states for boron and nitrogen doped systems become increasingly localized as the structure is dimensionally constrained from bulk → surface → layer → nanotube → nanorod. This may have important consequences for the photocatalytic activity of these more localized states in lower dimensional structures. On the other hand, this may be partially alleviated by having these states located on the structure's surface. In this way, electron-hole pairs need not travel significantly, as is the case for bulk materials.

### D. Energy Gaps

To analyze the qualitative trends in photocatalytic activity of boron and nitrogen doped $TiO_2$ nanostructures, we shall now compare the energy gaps obtained using different approximations within DFT, GW calculations, and experiment.

The DFT calculated energy gaps $\varepsilon_{gap}$, for $(TiO_2)_n$ clusters ($n \leq 9$) and band gaps for $TiO_2$ (2,2) nanorods, (3,3) nanotubes, and (4,4) nanotubes, in the undoped, boron doped, and nitrogen doped forms, are shown in Fig. 10. For the clusters, the gap is estimated by both the difference in energy between the HOMO and LUMO, and the difference between the ionization potential and electron affinity energies $I_p - E_a$. The band gap for $TiO_2$ nanorods, nanotubes, layers, surfaces and bulk phases is approximated by the indirect band gap between highest occupied and lowest unoccupied states. Although not as relevant for photoabsorption as the direct gap, the large size required for the doped super cells, shown in Fig. 6 and Fig. 9, leaves indirect and direct gaps indistinguishable. For the undoped nanorods and nanotubes and bulk rutile we find the band gap is direct, while for the undoped HexABC layer and anatase structures we find the band gap is indirect. For the same structures we also provide B3LYP band gaps, GW calculations, and experimental results for comparison.

As previous studies have shown, standard DFT tends to underestimate band gaps for bulk $TiO_2$ by approximately 1 eV, due in part to self-interaction errors [31, 32]. This may

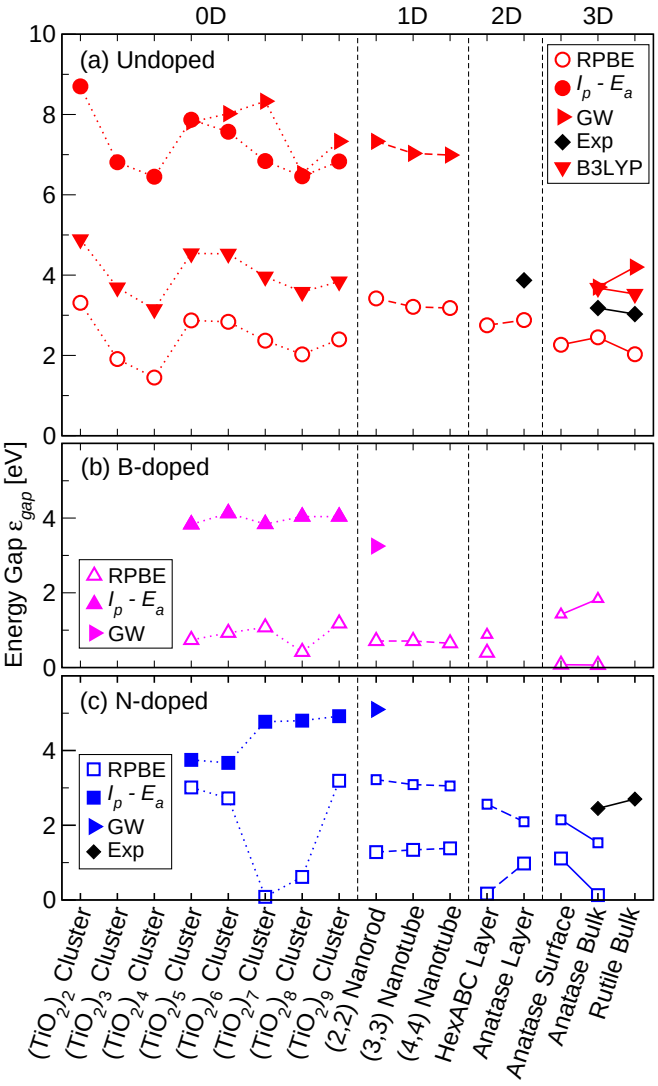



FIG. 10: Energy gap $\varepsilon_{gap}$ in eV versus $TiO_2$ structure for 0D $(TiO_2)_n$ clusters ($n \leq 9$), 1D $TiO_2$ (2,2) nanorods, (3,3) nanotubes, (4,4) nanotubes, 2D HexABC and anatase layers, and 3D anatase surface, anatase bulk, and rutile bulk phases. DFT calculations using RPBE of the highest occupied and lowest unoccupied state gaps / $I_p - E_a$ for the (a) undoped (○/●, red), (b) boron doped (△/▲, magenta), and (c) nitrogen doped (□/■, blue) systems are compared with undoped B3LYP (▼), GW (▶), and experimental ($u$) results [6, 12, 18, 30]. Small open symbols denote transitions between highest fully occupied states and the conduction band.

be partially addressed by the use of hybrid functionals such as B3LYP, which generally seem to improve band gaps for bulk systems [33–35]. However, B3LYP calculations for $TiO_2$ clusters largely underestimate the gap relative to the more reliable $I_p - E_a$, while for the bulks the gap is overestimated by approximately 0.4 eV relative to experiment. Also, B3LYP and RPBE calculations provide the same qualitative description of the *trends* in the energy gaps for $TiO_2$.

GW is probably the most successful and generally applicable method to calculate quasi-particle gaps. For clusters it agrees well with $I_p - E_a$, but for bulk systems GW seems to

overestimate the experimental gap like B3LYP. This overestimation by GW may be attributed to excitonic effects, which are not included in GW, or the role played by oxygen defects [36]. For these reasons, GW and DFT calculations are best used as upper and lower bounds for optical band gaps.

Fig. 10 shows that for both 3D and 2D systems, RPBE gaps underestimate the experimental results by approximately 1 eV. For 1D and 0D systems, we find a much larger difference of about 4 eV and 5 eV respectively, between the RPBE gaps and the $I_p - E_a$ and GW results. We may attribute this increasing disparity to the greater quantum confinement and charge localization in the 1D and 0D systems, which yield greater self-interaction effects. We find B3LYP gaps also underestimate this effect, simply increasing the RPBE energy gaps for both 0D and 3D systems up by about 1.4 eV.

On the other hand, we find the RPBE gaps reproduce qualitatively the structural dependence of the $I_p - E_a$, GW, and experimental results for a given dimensionality, up to a constant shift. This is true even for 3D bulk systems, where standard DFT does not predict rutile to be the most stable [29], as shown in Fig. 1.

Whether calculated using RPBE, $I_p - E_a$ or GW, the energy gaps for both boron and nitrogen doped $TiO_2$ nanostructures are generally narrowed, as shown in Fig. 10(b) and (c). However, for nitrogen doped $(TiO_2)_n$ clusters where nitrogen acts as an acceptor ($n = 5, 6, 9$), the energy gap is actually *increased* when spin is conserved, compared to the undoped clusters in RPBE. This effect is not properly described by the $N \to N + 1$ transitions of $I_p - E_a$, for which spin is not conserved for these nitrogen doped clusters. On the other hand, when nitrogen acts as a donor ($n = 7, 8$) the smallest gap between energy levels does conserve spin.

The boron doped $TiO_2$ nanorods and nanotubes have perhaps the most promising energy gap results of the $TiO_2$ structures considered herein, as seen in Fig. 5(b). Boron dopants introduce in the nanorods localized occupied states near the conduction band edge in both RPBE (*cf.* Figs. 5 and 6) and GW (*cf.* Fig. 7) calculations. On the other hand, nitrogen doping of nanorods and nanotubes introduces well defined mid-gap states, as shown in Fig. 5(c). However, to perform water dissociation, the energy of the excited electron must be above that for hydrogen evolution, with respect to the vacuum level. This is not the case for such a mid-gap state. This opens the possibility of a second excitation from the mid-gap state to the conduction band. However, the cross section for such an excitation may be rather low.

For boron doping of 2D and 3D structures, the highest occupied state donates its electron almost entirely to the conduction band, yielding an $n$-type semiconductor. Thus at very low temperatures, the RPBE band gap is very small. The same is true for $n$-type nitrogen doped bulk anatase. For these reasons, we also provide the energy gap between the highest fully occupied state and the conduction band, which may be more relevant for photoabsorption. We find these RPBE gaps are still generally smaller than those for their undoped $TiO_2$ counterparts.

In summary, for both boron and nitrogen doped clusters we find RPBE gaps differ from $I_p - E_a$ by about 3 eV, while for nitrogen doped anatase the RPBE gap differs from experiment by about 0.6 eV. Given the common shift of 1 eV for undoped 2D and 3D structures, this suggests that both boron and nitrogen doped 2D $TiO_2$ structures are promising candidates for photocatalysis. Further, the boron and nitrogen doped 1D nanotube results also warrant further experimental investigation.

## V. CONCLUSION

In conclusion, we have demonstrated how the electronic properties of $TiO_2$ may be "tailored" using nanostructural changes in combination with boron and nitrogen doping. While boron doping tends to produce smaller band gap $n$-type semiconductors, nitrogen doping produces $p$-type or $n$-type semiconductors depending on whether or not nearby oxygen atoms occupy surface sites. This suggests that a $p$-type $TiO_2$ semiconductor may be produced using nitrogen doping in conjunction with surface confinement at the nanoscale.

### Acknowledgments

We thank S. In, Z.-W. Qu, G.-J. Kroes, T. Jaramillo, and J. K. Nørskov for useful discussions. The authors acknowledge financial support from NABIIT and the Danish Center for Scientific Computing. J.I.M. acknowledges the financial support of the STREP EU APOLLON-B Project through grant No. NMP3-CT-2006-033228. The Center for Atomic-scale Materials Design (CAMD) is sponsored by the Lundbeck Foundation.

[1] A. Heller, "Hydrogen-evolving solar cells", Science **223**(4641), 1141 (Mar. 1984), doi:10.1126/science.223.4641.1141.

[2] M. Grätzel, "Photoelectrochemical cells", Nature **414**(6861), 338 (Nov. 2001), doi:10.1038/35104607.

[3] M. R. Hoffmann, S. T. Martin, W. Y. Choi, and D. W. Bahnmann, "Environmental applications of semiconductor photocatalysis", Chem. Rev. **95**(1), 69 (Jan. 1995), doi:10.1021/cr00033a004.

[4] S. U. M. Khan, M. Al-Shahry, and W. B. Ingler, "Efficient photochemical water splitting by a chemically modified n-$TiO_2$", Science **297**(5590), 2243 (Sep. 2002), doi:10.1126/science.1075035.

[5] Y. Gai, J. Li, S.-S. Li, J.-B. Xia, and S.-H. Wei, "Design of narrow-gap $TiO_2$: A passivated codoping approach for enhanced photoelectrochemical activity", Phys. Rev. Lett. **102**(3), 036402 (Jan. 2009), doi:10.1103/PhysRevLett.102.036402.

[6] Z.-W. Qu and G.-J. Kroes, "Theoretical study of the electronic structure and stability of titanium dioxide clusters $(TiO_2)_n$ with $n$ = 1–9", J. Phys. Chem. B **110**, 8998 (Apr. 2006), doi:10.1021/jp056607p.

[7] H.-J. Zhai and L.-S. Wang, "Probing the electronic structure and band gap eveolition of titanium oxide clusters $(TiO_2)_n^-$ ($n$ = 1–10) using photoelectron spectroscopy", J. Amer. Chem. Soc. **129**(10), 3022 (Feb. 2007), doi:10.1021/ja068601z.

[8] H. Imai, Y. Takei, K. Shimizu, M. Matsuda, and H. Hirashima, "Direct preparation of anatase $TiO_2$ nanotubes in porous alumina membranes", J. Mater. Chem. **9**(12), 2971 (Oct. 1999), doi:10.1039/a906005g.

[9] T. Kasuga, M. Hiramatsu, A. Hoson, T. Sekino, and K. Niihara, "Titania nanotubes prepared by chemical processing", Adv. Mater. **11**(15), 1307 (Oct. 1999), doi:10.1002/(SICI)1521-4095(199910)11:15¡1307::AID-ADMA1307¿3.0.CO;2-H.

[10] G. Mogilevsky, Q. Chen, H. Kulkarni, A. Kleinhammes, W. M. Mullins, and Y. Wu, "Layered nanostructures of delaminated anatase: Nanosheets and nanotubes", J. Phys. Chem. C **112**(9), 3239 (Feb. 2008), doi:10.1021/jp076899p.

[11] S. In, A. Orlov, R. Berg, F. Carcía, S. Pedrosa-Jimenez, M. S. Tikhov, D. S. Wright, and R. M. Lambert, "Effective visible light-activated B-doped and B,N-codoped $TiO_2$ photocatalysts", J. Amer. Chem. Soc. **129**(45), 13790 (Oct. 2007), doi:10.1021/ja0749237.

[12] G. Liu, F. Li, D.-W. Wang, D.-M. Tang, C. Liu, X. Ma, G. Q. Lu, and H.-M. Cheng, "Electron field emission of a nitrogen-doped $TiO_2$ nanotube array", Nanotechnology **19**(2), 025606 (Jan. 2008), doi:10.1088/0957-4484/19/02/025606.

[13] R. Asahi, T. Morikawa, T. Ohwaki, K. Akoki, and Y. Taga, "Visible-light photocatalysis in nitrogen-doped titanium oxides", Science **298**(5528), 269 (Jul. 2001), doi:10.1126/science.1061051.

[14] A. Ghicov, J. M. Macak, H. Tsuchiya, J. Kunze, V. Hæublein, S. Kleber, and P. Schmuki, "$TiO_2$ nanotube layers: Dose effects during nitrogen doping by ion implantation", Chem. Phys. Lett. **419**(4–6), 426 (Feb. 2006), doi:10.1016/j.cplett.2005.11.102.

[15] Y. Chen, S. Zhang, Y. Yu, H. Wu, S. Wang, B. Zhu, W. Huang, and S. Wu, "Synthesis, characterization, and photocatalytic activity of N-doped $TiO_2$ nanotubes", J. Disp. Sci. Tech. **29**(2), 245 (Feb. 2008), doi:10.1080/01932690701707456.

[16] A. Nambu, J. Graciani, J. A. Rodriguez, Q. Wu, E. Fujita, and J. F. Sanz, "N doping of $TiO_2$(110): Photoemission and density-functional studies", J. Chem. Phys. **125**(9), 094706 (Sep. 2006), doi:10.1063/1.2345062.

[17] J. Graciani, L. J. Álvarez, J. A. Rodriguez, and J. F. Sanz, "N doping of rutile $TiO_2$(110) surface. a theoretical DFT study", J. Phys. Chem. C **112**(7), 2624 (Jan. 2008), doi:10.1021/jp077417c.

[18] D. V. Bavykin, J. M. Friedrich, and F. C. Walsh, "Protonates titanates and $TiO_2$ nanostructured materials: Synthesis, properties, and applications", Adv. Mater. **18**(21), 2807 (Oct. 2006), doi:10.1002/adma.200502696.

[19] O. Khaselev and J. A. Turner, "A monolithic photovoltaic-photoelectrochemical device for hydrogen production via water splitting", Science **280**(5362), 425 (Apr. 1998), doi:10.1126/science.280.5362.425.

[20] B. Hammer, L. B. Hansen, and J. K. Norskov, "Improved adsorption energetics with density functional theory using revised Perdew-Burke-Ernzerhof functionals", Phys. Rev. B **59**(11), 7413 (Mar. 1999), doi:10.1103/PhysRevB.59.7413.

[21] URL wiki.fysik.dtu.dk/dacapo.

[22] S. R. Bahn and K. W. Jacobsen, "An object-oriented scripting interface to a legacy electronic structure code", Comput. Sci. Eng. **4**(3), 56 (May 2002), doi:10.1109/5992.998641.

[23] M. Marques, A. Castro, G. F. Bertsch, and A. Rubio, "`octopus`: A first-principles tool for excited electron-ion dynamics", Comput. Phys. Commun. **151**(1), 60 (Mar. 2003), URL www.tddft.org/programs/octopus, doi:10.1016/S0010-4655(02)00686-0.

[24] A. Marini, C. Hogan, M. Grüning, and D. Varsano, "`yambo`: An *ab initio* tool for excited state calculations", Comp. Phys. Comm. **180**(8), 1392 (Aug. 2009), URL www.yambo-code.org, doi:10.1016/j.cpc.2009.02.003.

[25] X. Gonze, J.-M. Beuken, R. Caracas, F. Detraux, M. Fuchs, L. S. G.-M. Rignanese, M. Verstraete, G. Zerah, F. Jollet, M. Torrent, A. Roy, M. Mikami, P. Ghosez, J.-Y. Raty, and D. Allan, "First-principles computation of material properties: the ABINIT software project", Comp. Mater. Sci. **25**(3), 478 (Nov. 2002), URL www.abinit.org.

[26] S. Baroni, A. D. Corso, S. de Gironcoli, P. Giannozzi, C. Cavazzoni, G. Ballabio, S. Scandolo, G. Chiarotti, P. Focher, A. Pasquarello, K. Laasonen, A. Trave, R. Car, N. Marzari, and A. Kokalj, "Quantum-espresso package" (2005), URL www.quantum-espresso.org/.

[27] D. Lide, *Handbook of Chemistry and Physics*, 87th ed. (CRC-Press, 2006–2007).

[28] A. N. Enyashin and G. Seifert, "Structure, stability and electronic properties of $TiO_2$ nanostructures", Phys. Stat. Sol. B **242**(7), 1361 (May 2005), doi:10.1002/pssb.200540026.

[29] F. Labat, P. Baranek, C. Doman, C. Minot, and C. Adamo, "Density functional theory analysis of the structural and electronic properties of $TiO_2$ rutile and anatase polytypes: Performances of different exchange-correlation functionals", J. Chem. Phys. **126**(15), 154703 (Apr. 2007), doi:10.1063/1.2717168.

[30] L. Thulin and J. Guerra, "Calculations of strain-modified anatase $TiO_2$ band structures", Phy. Rev. B **77**(19), 195112 (May 2008), doi:10.1103/PhysRevB.77.195112.

[31] Z.-L. Cai, K. Sendt, and J. R. Reimers, "Failure of density-functional theory and time-dependent density-functional theory for large extended $\pi$ systems", J. Chem. Phys **117**(12), 5543 (Sep. 2002), doi:10.1063/1.1501131.

[32] U. Salzner, J. B. Lagowski, P. G. Pickup, and R. A. Poirier, "Design of low band gap polymers employing density functional theory – hybrid functionals ameliorate band gap problem", J. Comput. Chem. **18**(15), 1943 (Nov. 1997), doi:10.1002/(SICI)1096-987X(19971130)18:15¡1943::AID-JCC9¿3.0.CO;2-O.

[33] J. Muscat, A. Wander, and N. M. Harrison, "On the prediction of band gaps from hybrid functional theory", Chem. Phys. Lett. **342**(3–4), 397 (Jul. 2001), doi:10.1016/S0009-2614(01)00616-9.

[34] F. D. Angelis, A. Tilocca, and A. Selloni, "Time-dependent dft study of $[Fe(CN)_6]^{4-}$ sensitization of $TiO_2$ nanoparticles", J. Amer. Chem. Soc. **126**(46), 15024 (Oct. 2004), doi:10.1021/ja045152z.

[35] C. D. Valentin, G. Pacchioni, and A. Selloni, "Electronic structure of defect states in hydroxylated and reduced rutile $TiO_2$(110) surfaces", Phys. Rev. Lett. **97**(16), 166803 (Oct. 2006), doi:10.1103/PhysRevLett.97.166803.

[36] P. J. Hardmand, G. N. Raikar, C. A. Muryn, G. van der Laan, P. L. Wincott, G. Thornton, D. W. Bullett, and P. A. D. M. A. Dale, "Valence-band structure of $TiO_2$ along the $\Gamma$-$\Delta$-$X$ and $\Gamma$-$\Sigma$-$M$ directions", Phys. Rev. B **49**(11), 7170 (Mar. 1994), doi:10.1103/PhysRevB.49.7170.